

# Soft Matter

Accepted Manuscript

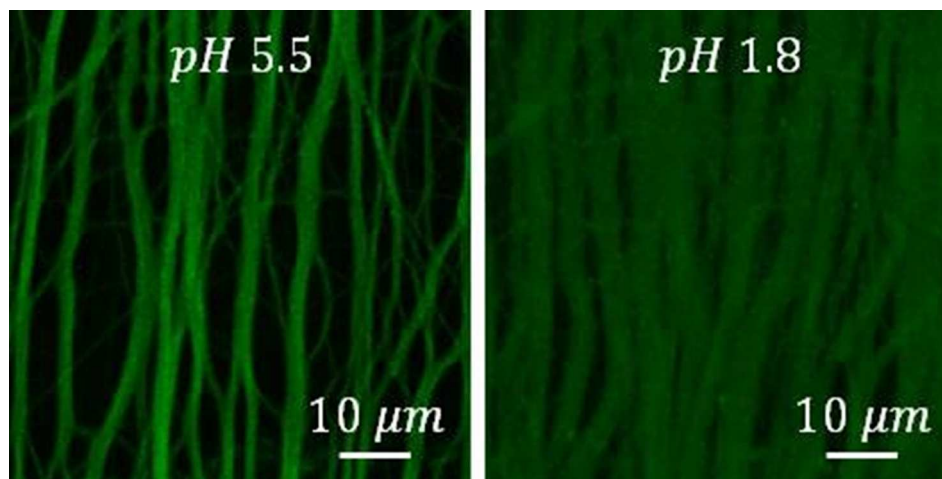


This is an *Accepted Manuscript*, which has been through the Royal Society of Chemistry peer review process and has been accepted for publication.

*Accepted Manuscripts* are published online shortly after acceptance, before technical editing, formatting and proof reading. Using this free service, authors can make their results available to the community, in citable form, before we publish the edited article. We will replace this *Accepted Manuscript* with the edited and formatted *Advance Article* as soon as it is available.

You can find more information about *Accepted Manuscripts* in the [Information for Authors](#).

Please note that technical editing may introduce minor changes to the text and/or graphics, which may alter content. The journal's standard [Terms & Conditions](#) and the [Ethical guidelines](#) still apply. In no event shall the Royal Society of Chemistry be held responsible for any errors or omissions in this *Accepted Manuscript* or any consequences arising from the use of any information it contains.



80x39mm (150 x 150 DPI)

Cite this: DOI: 10.1039/c0xx00000x

www.rsc.org/xxxxxx

ARTICLE TYPE

# Electrospinning Polyelectrolyte Complexes: pH-Responsive Fibers

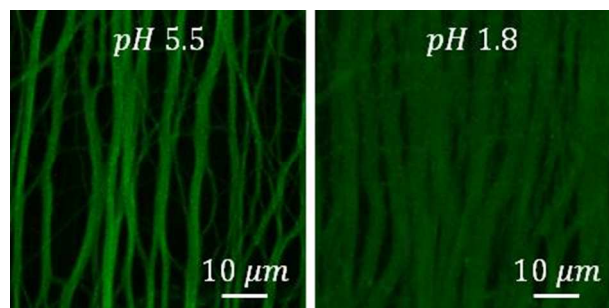
Mor Boas,<sup>\*a</sup> Arkadiusz Gradys,<sup>b</sup> Gleb Vasilyev,<sup>c</sup> Michael Burman,<sup>c</sup> and Eyal Zussman<sup>a,c</sup>

Received (in XXX, XXX) Xth XXXXXXXXX 20XX, Accepted Xth XXXXXXXXX 20XX

DOI: 10.1039/b000000x

Fibers were electrospun from a solution comprised of oppositely charged polyelectrolytes, in efforts to achieve highly confined macromolecular packaging. A stoichiometric ratio of poly(allylamine hydrochloride) and poly(acrylic acid) solution was mixed in a water/ethanol co-solvent. Differential scanning calorimetry (DSC) analysis of electrospun fibers demonstrated no indication of glass transition,  $T_g$ . Infrared spectroscopy (FTIR) analysis of the fibers as a function of temperature, demonstrated an amidation process at lower temperature compared to cast film. Polarized FTIR indicated a preference of the functional groups to be perpendicular to the fiber axis. These results imply formation of mixed phase fibers with enhanced conditions for intermolecular interactions, due to the highly aligned and confined assembly of the macromolecules. The tunable intermolecular interactions between the functional groups of the polyelectrolytes, impact pH-driven, reversible swelling-deswelling of the fibers. The degree of ionization of PAA at pH 5.5 and pH 1.8 varied from 85% to 18%, correspondingly, causes transformation of ionic interactions to hydrogen bonding between the functional groups. The chemical change led to massive water diffusion of 500% by weight and to a marked increase of 400% in fiber diameter, at a rate of 0.50  $\mu\text{m/s}$ . These results allow for manipulation and tailoring of key fiber properties for tissue engineering, membranes, and artificial muscle applications.

For table of content



## 1. Introduction

Polyelectrolyte complexes are the association complexes formed between oppositely charged polyelectrolytes.<sup>1</sup> Electrostatic interactions between the polyelectrolytes and increased entropy resulting from counter-ion release, are the driving forces for such complexation.<sup>2</sup> The formation of such complexes is affected by many factors, including polymer molecular weight and concentration, and solution ionic strength and pH. The morphology of polyelectrolyte complexes is dictated by molecular weight, solvent, and ionic strength, and takes on either the ladder-like, or the “scrambled egg” configuration.<sup>3-5</sup> The ladder-like model assumes that the chains are flexible enough for high interaction between them to zip together. In the more common scrambled egg configuration, oppositely charged units form ion pairs, however the chains are randomly mixed (tangled) in a globular fashion.

The assembly method employed to prepare polyelectrolyte complexes can largely impact their tunable properties. The layer-by-layer (LbL) method, in which sequential adsorption and deposition of oppositely charged polyelectrolytes occur, provides a unique combination of the polyelectrolyte complex properties due to the ionically cross-linked nature of the thin multilayer assembly.<sup>6,7</sup> Owing

to the simplicity of its use and modification, the method can be applied on different surfaces and structures, and supports addition of a variety of materials or different polymers to the assembly.<sup>8</sup>

Electrospinning is an alternative single-step assembly method for fabrication of nano-scale polyelectrolyte complex-based fibers. In this method, a polymer solution, typically semidilute, is extruded from a spinneret by a strong electric field. Once a cone-jet mode is established, a fluid jet is emitted from the conical tip.<sup>9, 10</sup> The jet undergoes extreme elongation and thinning, concurrent with rapid solvent evaporation, resulting in quenching of the polymer matrix macrostructure in a non-equilibrium state. In-process electrospinning measurements show that the polymer macromolecules are stretched along the jet.<sup>11, 12</sup> In addition, molecular dynamics simulation,<sup>13</sup> and experimental results<sup>14-16</sup> detected highly confined macromolecules in the electrospun fibers, which imply geometrical constraint. Such a molecular arrangement may enhance availability for intermolecular interactions when electrospun polymer solution consists of oppositely charged polyelectrolytes.

Poly(acrylic acid) (PAA) and poly(allylamine hydrochloride) (PAH) are weakly charged polyelectrolytes (Figure 1), that form complex under low salt concentrations and neutral pH.<sup>1</sup> These polyelectrolytes can be applied in a wide range of technologies, such as drug delivery, encapsulation<sup>17</sup> and three-dimensional writing ink.<sup>18</sup>

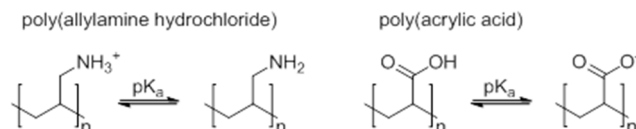


**Figure 1:** Chemical structure of poly(acrylic acid) (PAA) and poly(allylamine hydrochloride) (PAH) under different pH levels.

Chemical changes in functional groups of PAA and PAH (amine and carboxylic acid) drive polyelectrolyte complexation. Under neutral pH, the amine is protonated to ammonium and the carboxylic acid is deprotonated to carboxylate. Local ionic  $\text{NH}_3^+ \text{-COO}^-$  crosslinks can then be generated and polyelectrolyte complexes are formed.<sup>19</sup> However, the polyelectrolyte complex only remains stable under constrict conditions. At low pH, the ammonium and carboxylic acid can no longer form ionic interactions but only hydrogen bonds, thus the disordered nature of spontaneous complexation leads to disassembly and dissolution of PAA and PAH macromolecules. Characterizing the flexibility-or stiffness-of those macromolecules is of basic importance for describing their structure and dynamics. The persistence length of single chain of PAA and PAH, at low pH (range of 0-4) is nearly constant, 4Å for PAA and 12Å for PAH due to higher repulsion forces between ammonium groups which affects the rigidity.<sup>20</sup> In semidilute solution of mixed polyelectrolytes, the mesh size which is influenced by the chain-chain interactions and the charge screening between the oppositely charged macromolecules affects the behaviour of the polyelectrolytes.<sup>21</sup> If the persistence length is smaller than the mesh size, the polyelectrolyte solution behaves as a neutral semiflexible polymer solution.<sup>22</sup>

When using the LbL assembly method, there has been much experimental research on the fabrication and structure of PAA and PAH complex and their respective functional groups.<sup>19, 23-26</sup> The exact mechanisms underlying the formation of nanoscale films/composites is not yet fully clear, although a model of highly entangled and interpenetrated inner multilayer structure has been proposed.<sup>27</sup> Computational calculations have suggested that short fragments arranged in a ladder-like alignment,<sup>28</sup> secure the stability of the PAA and PAH complex. The LbL assembly can undergo a balance of electrostatics and hydrogen bonding, facilitating the development of tunable materials that exhibit swelling behavior in response to external stimuli.<sup>19</sup> When applying the electrospinning process, the strong elongational flow along the electrospinning jet is expected to transform the initial equilibrium state of the PAA and PAH network to an almost fully stretched state along the jet. This stretching is accompanied by network contraction across<sup>29</sup> the jet (see Figure 2a). Furthermore, assuming that the macromolecules are highly confined and oriented along the electrospun fibers, the repulsive nature of polyelectrolytes in solution should increase their persistence length and rigidity,<sup>20</sup> resulting in fibers with a higher degree of confinement than neutral polymers.<sup>16</sup> Since the torsional angle of the functional groups of the polyelectrolytes has high rotational freedom perpendicular to the chain's axis, as reported for PAA,<sup>30</sup> the functional groups can rotate to the angle optimal for interacting with each other (see Figure 2b). It must be noted that not all charges are free to interact, likely due to a conformational and steric constraints.<sup>31</sup>

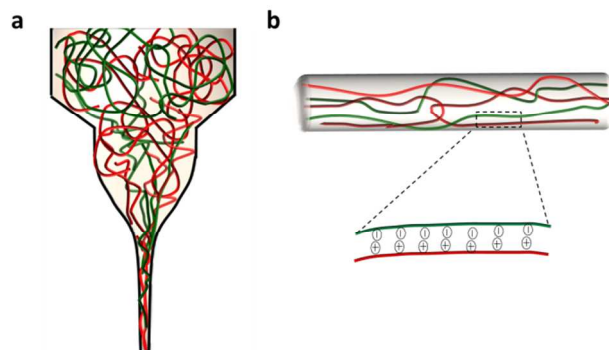


**Figure 2:** Schematic illustration of the experimental setup for electrospinning of PAA and PAH and resultant as-spun fibers. (a) Stretched macromolecules in the jet in the vicinity of the Taylor cone. (b) Schematic illustration of packing of the aligned macromolecules in the electrospun fiber.

We hypothesize that when electrospun PAA/PAH fibers are immersed in water, the chemical response of the functional groups will favor either hydrogen bonds or ionic interactions, in accordance with the pH of the medium. Highly confined macromolecules featuring potential intermolecular interaction sites, will enable extensive swelling behavior. At low pH, the functional groups are almost fully protonated, resulting in ionic repulsion between charged ammonium groups, hydrogen bonds between ammonium and carboxylic acid, and water molecules diffusion to form hydrogen bonds. At neutral pH, the highly confined structure will maximize cohesion between the two components and minimize diffusion of water molecules into the fibers.

This paper presents fabrication of PAA/PAH electrospun fibers under various conditions. Fiber morphology and orientation of the polyelectrolytes are analysed, followed by a study of the thermal and chemical behavior of the fibers as compared to cast film. The swelling performance of the electrospun polyelectrolyte complex-based fibers is assessed, with focus on both time dependence and the degree of ionization of the functional groups along with the acid dissociation constant (pKa).

## 2. EXPERIMENTAL SECTION

### 2.1 Materials

PAH ( $M_w=120,000-180,000 \text{ g mol}^{-1}$ ) was purchased from Polyscience Inc. (Niles, Illinois), and PAA ( $M_w=120,000-180,000 \text{ g mol}^{-1}$ ) and ethanol were purchased from Sigma-Aldrich; all three reagents were used as received. The solutions were prepared with purified water with a resistivity of  $18.2 \text{ M}\Omega \text{ cm}$  (Bronstead purification system).

A mixture of PAA and PAH, at molar ratio 1:1 (by repeating unit), was dissolved in an ethanol/water mixture and stirred overnight. The ethanol concentration in the co-solvent was 0, 20, 40 or 60 % (v/v). Total polymer concentration in solutions was 10.3 % (w/w).

### 2.2 Methods

#### 2.2.1 Electrospinning and film preparation

Homogenous PAA/PAH solutions were electrospun to form fiber mats of oriented nanofibers. The flow rate, controlled by a syringe pump (pump 11 elite, Harvard apparatus), of the PAA/PAH solution was constant ( $0.7 \text{ mL/h}$ ), with an electrostatic field of  $0.85 \text{ kV/cm}$ . A collector wheel, with a tangential velocity of  $6 \text{ m/s}$  and positioned at a distance of  $10 \text{ cm}$  from the spinneret (needle 23G), was used to collect the aligned fibers.<sup>32</sup> The films were prepared by casting the PAA/PAH solution onto a square Teflon mold ( $40 \text{ mm}$  long,  $2 \text{ mm}$  deep) and then air-drying them for three days, followed by overnight vacuum. PAA/PAH film and fibers were dried at  $90 \text{ }^\circ\text{C}$  for  $1 \text{ h}$  prior to any measurements.

#### 2.2.2 Sample Characterization

Images of the as-spun and dried fibers were obtained, using a scanning electron microscopy (FEI E-SEM Quanta 200), at an acceleration voltage of  $2-4 \text{ kV}$  and sample-to-detector distance of  $2-5 \text{ mm}$ . The specimens were coated with a thin gold film prior to analysis.

Thermal behavior of the fibers and films was investigated using a differential scanning calorimeter (STARe DSC, Mettler-Toledo), set at a heating rate of  $10 \text{ }^\circ\text{C/min}$ . The DSC was calibrated for temperature and heat flow using indium and zinc standards. Measurements were conducted under nitrogen purge set at  $50 \text{ ml min}^{-1}$ .

The chemical structure of the fibers and films was investigated by attenuated total reflectance Fourier transform infrared spectroscopy (ATR-FTIR, Thermo, Nicolet 380) and was scanned over a range of  $500$  up to  $4000 \text{ cm}^{-1}$ , at a resolution of  $2 \text{ cm}^{-1}$ . Measurements were performed at room temperature, on samples heated in the DSC cell to temperatures within their thermal transition ranges.

In order to monitor the changes in the molecular orientation along and perpendicular to the fiber's axis, FTIR (Thermo, Nicolet 8700) with a ZnSe polarizer was conducted.

For evaluation of the degree of ionization of PAA in the PAA/PAH fibers, spectrum collection using FTIR-ATR of fibers immersed in aqueous solutions at varied pH levels was performed. The spectra were analyzed using Origin software. Due to overlapping of the PAH peaks, deconvolution of the COOH band ( $1709 \text{ cm}^{-1}$ ) and COO<sup>-</sup> ( $1557 \text{ cm}^{-1}$ ) was conducted. Assuming the same extinction coefficient for both bands,<sup>33</sup> the degree of ionization of PAA at given pH was calculated as  $\alpha=(\text{peak area of COO}^-)/(\text{peak area of COOH}+\text{peak area of COO}^-)$ .

A confocal laser scanning microscope (CSLM, Zeiss LSM510) was used for in-situ imaging in water. Plan-view images of the fibers were collected at each height scan, using a  $63\times$  water immersion objective lens. For illustration purposes, ImageJ software was applied to construct plan-view images from the CSLM images (see Supplementary Material for further details).

The dependence of water diffusion competence on pH was evaluated by measuring water content in the fiber mats. The dry fiber mat was weighed immediately after drying, followed by alternating immersion in water at pH 5.5 and then at pH 1.8, for 10 minutes in each pH. Finally, the fiber mat was removed from the water bath, dried and weighed.

Imaging of single electrospun fibers, and single fibers immersed in water of different pH values, was conducted at room-temperature and under a cryogenic-temperature high resolution-scanning electron microscope (RT HR-SEM and cryo-HR-SEM) to avoid wrinkling as expected by wetting hydrogel in water<sup>34</sup> (see Supplementary Material for further details). In all cases, the uncoated specimens were imaged at a short working distance of  $3-3.5 \text{ mm}$ , at a low accelerating voltage of  $0.7-1 \text{ kV}$ , using a combination of two secondary electron detectors: the Everhart-Thornley detector and the high-resolution in-the-column detector.

#### 2.2.3 Swelling measurements

A sample of a free-standing electrospun  $20\mu\text{m}$ -wide fiber mat was mounted on epoxy resin-based protrusions located on a glass substrate (see Figure 3a). The glass substrate was adhered to glass tubing with an in- and out-flow to allow pH change of the medium. The fiber mat was observed with an optical microscope during pH manipulations (see Figure 3b). Swelling measurements were recorded between

bumps.

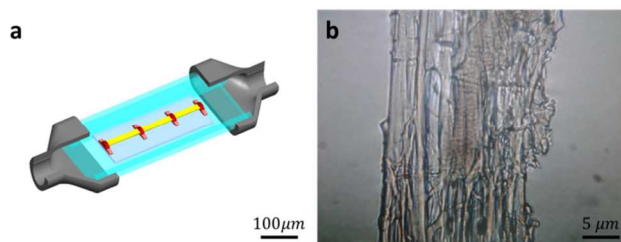


**Figure 3:** (a) A sketch of the swelling measurement set-up. Epoxy bumps were spaced at intervals of approximately 100  $\mu\text{m}$ . (b) A typical example of the fiber mat as observed under the optical microscope (see Supplementary information for a video demonstrating the swelling process).

5

### 3. Results and discussion

#### 3.1 Electrospinning

In order to achieve a stable structure with enhanced responsive behavior, a stoichiometric ratio between the oppositely charged functional groups is necessary. This ratio assists in minimizing free energy during the rapid stretching of PAA and PAH, and secures the most favorable complex between the macromolecules.<sup>5, 35</sup> However, a 1:1 ratio of oppositely charged polyelectrolytes tends to precipitate in water due to electrostatic interactions. When the solution is adjusted to low pH, PAH is mostly ionized and PAA is not mostly ionized with lower calculated persistence length than PAH.<sup>20</sup> The high proportion of protonated functional groups reduce the electrostatic interactions between PAA and PAH.<sup>20, 36</sup> However, electrospinning occurred during attempts to fabricate fibers from a stoichiometric ratio (by repeating unit) of PAA/PAH in water (see Figure 4). In efforts to stabilize the jet, the rheology and polarity of the solution were tuned. Addition of ethanol as a co-solvent, at ratio of 40:60 with water, increased the relative shear viscosity of PAA/PAH by  $\sim 200\%$  [see supporting information for rheological measurements]. In addition, the ethanol also reduced the polarity of the aqueous solution, resulting in restraint of unbalanced charging and in jet stabilization. Resultant fibers feature a diameter range of 300-600 nm, and were non-porous, and partially buckled<sup>34</sup> (Figure 5).

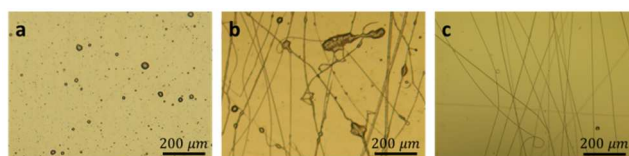


**Figure 4:** Light field optical microscope images of the electrospinning process. A 10.3% PAA/PAH solution prepared with (a) water as solvent, (b) 20:80 ethanol/water as co-solvent, or (c) 40:60 ethanol/water as co-solvent.

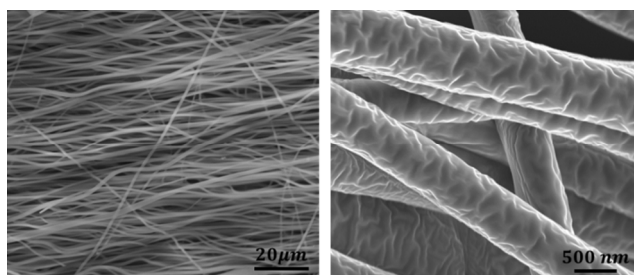


**Figure 5:** SEM images of electrospun fibers following subsection to 90  $^{\circ}\text{C}$  (1 h) and high pressure vacuum, at different magnifications.

25

#### 3.2 Thermal and chemical properties of electrospun fibers

In order to demonstrate the influence of the assembly method on the complexation process, thermal behavior of PAA/PAH fibers were compared to cast PAA/PAH films. DSC heating scans, registered up to 450  $^{\circ}\text{C}$ , of PAA/PAH as cast film and as-spun fibers, stored at ambient conditions, showed several endothermic peaks (not presented), starting with a broad peak located in the range 50–150  $^{\circ}\text{C}$ . This first peak relates to evaporation of physically absorbed water, as previously reported<sup>37</sup> and as further confirmed by FTIR. We found that applying a first cycle of heating the samples at 90  $^{\circ}\text{C}$  for one hour prior to second run, yielded dry samples, whose thermal transitions without the water evaporation peak were detectable on the heating scans (Figure 6). This method may further be used in thermal investigation of PAA/PAH assemblies.

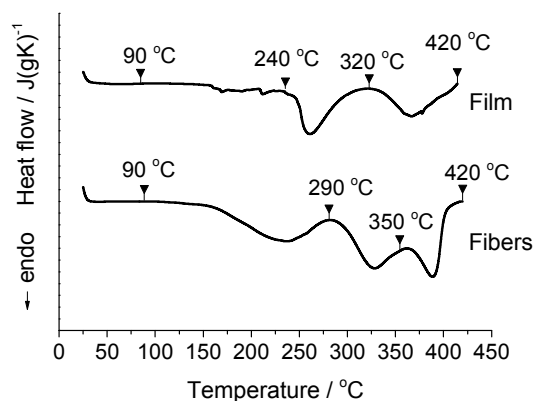


**Figure 6:** DSC heating scans registered at  $10 \text{ Kmin}^{-1}$  for PAA/PAH electrospun fiber mats and cast films. Marked are temperatures at which FTIR measurements were performed (see Figure 7).

While a heating scan of cast film registered only two endothermic peaks (260 and  $360 \text{ }^\circ\text{C}$ ), heating scans obtained for fibers contained three distinct endothermic peaks, a broad peak at  $200\text{--}300 \text{ }^\circ\text{C}$  and a double peak within the  $300\text{--}450 \text{ }^\circ\text{C}$  range. The position and size of the peaks strongly depended on the humidity during electrospinning process. Since no glass transition was recorded for either of the individual polyelectrolytes in the DSC scans, it can be argued that PAA and PAH form a mixed phase in the fibers.<sup>25</sup>

In order to reveal transitions related to the endothermic peaks evidenced by DSC, FTIR-ATR measurements were performed on cast films and fibers (see Figure 7). Upon drying the fiber mat at  $90 \text{ }^\circ\text{C}$ , a prominent peak ascribed to  $\text{C}=\text{O}$  stretching ( $1709 \text{ cm}^{-1}$ ) and asymmetric  $-\text{NH}_3^+$  ( $1595 \text{ cm}^{-1}$ ), was observed (see Table 1). No evidence for  $\text{COO}^-$  stretching was seen, since the pH of the solution was low,<sup>26</sup> most of the carboxylic acid and amine side-groups were protonated, as expected. The FTIR-ATR spectra of fibers heated to  $290 \text{ }^\circ\text{C}$  demonstrated two processes occurring in parallel: (1) Anhydride formation: The peak at  $1709 \text{ cm}^{-1}$  shifted to  $1716 \text{ cm}^{-1}$  ( $\text{C}=\text{O}$  stretching) upon heating. Similar behavior observed during thermal investigation of homopolymer PAA, was attributed to anhydride formation.<sup>37</sup> Appearance of peaks at  $1805$ ,  $1758$  and  $1045 \text{ cm}^{-1}$  also indicate the formation of anhydride. (2) Amidation: amine and carboxylic acid peaks ( $1604 \text{ cm}^{-1}$  and  $1716 \text{ cm}^{-1}$ , respectively) decreased and a new peak was observed at  $1660 \text{ cm}^{-1}$  (carbonyl stretching in CONH amide),<sup>38</sup> suggesting that the charged amine and carboxylic acid form intermolecular amide bonds in the fiber.

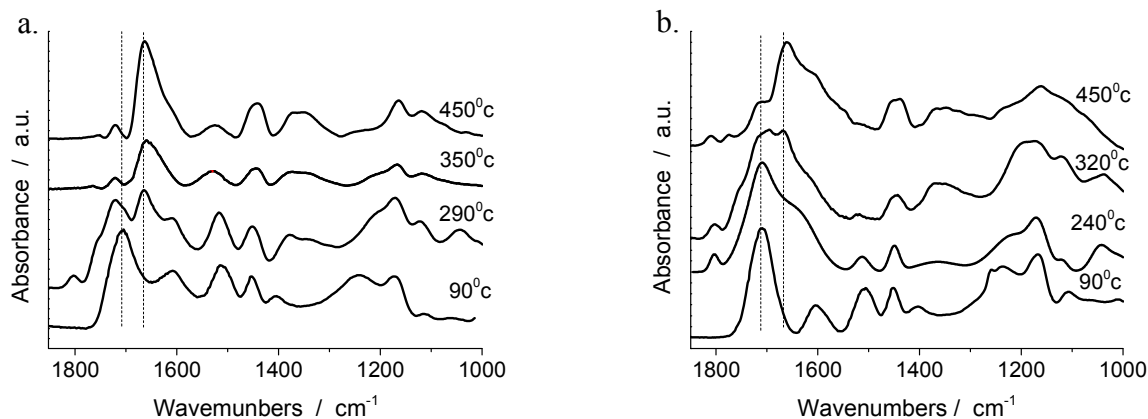


**Figure 7:** FTIR-ATR spectra of PAA/PAH fibers (a) and cast films (b), heated to the indicated temperatures

Extensive heating to  $350 \text{ }^\circ\text{C}$  (second DSC endothermic peak) was associated with extensive amidation. The amine-related peak was not observed and the intensity of the peak at  $1716 \text{ cm}^{-1}$  (carboxylic acid) decreased, as did the anhydride peaks. The intensity of the amide peak increased, suggesting that new amide bonds were formed from anhydride and amine functional groups. Heating to  $450 \text{ }^\circ\text{C}$  (end of the third endothermic peak) yielded signs of the beginning of fiber decomposition.

25

30

**Table 1:** ATR-FTIR band assignments.<sup>25, 37, 39</sup>

Assignment	Wavenumber (cm <sup>-1</sup> )
Ketone	1150
CO stretch	1230-1270
COH in plane deformation	1415
CH <sub>2</sub>	1452
NH bending vibrations	1600
Amide I band	1660
COOH stretch	1705-1720
COC anhydride	1045, 1758, 1805

DSC scanning of cast film yielded two major endothermic peaks after anhydride formation (see Figure 7b). The first peak (located at 260 °C) was related to amidation. The second peak withheld continuation of amidation, as found by FTIR, and the initiation of PAA decomposition. The transitions are in agreement with previous results.<sup>25</sup>

When comparing thermal behavior of fibers versus cast film, it becomes apparent that fiber amidation is detected in lower and broader peaks (150-290 cm<sup>-1</sup>) when compared with cast film (240-320 cm<sup>-1</sup>), namely, a lower energetic barrier must be surpassed for the interaction between the two polyelectrolytes to occur. This may indicate better confinement of the polyelectrolytes in the fiber, enabling interactions between the functional groups. Anhydride formation is not affected by structural factors, since it involves only PAA and occurs in parallel to amidation at the same temperature range. In contrast, decomposition may be affected by material structure and composition, as suggested by the different decomposition profiles when compared to those of the individual constituent polymers.

### 3.3 Orientational analysis

To study the orientation of the macromolecules, polarized FTIR absorption spectroscopy was performed on uniaxial fiber mats heated to 320 °C for 1 hour to increase amide peak intensity (see Figure 8). Spectra were collected with the incident light polarization parallel and perpendicular to the fiber axis. The curves are evidence to preferential absorption of light polarized perpendicular to the fiber axis. In particular, the polarized peak intensities of carboxylic acid, amide, and C-H stretching at 1716, 1660, and 1450 correspondingly, demonstrate that the functional groups are oriented perpendicular to the fiber axis. These observations suggest that PAA and PAH macromolecules are roughly stretched and oriented along the fiber axis, allowing intermolecular interactions to occur perpendicular to the fiber axis. The confined assembly of electrospun fibers leads to a lower energetic barrier for amidation than in cast film, as observed in the thermal analysis.

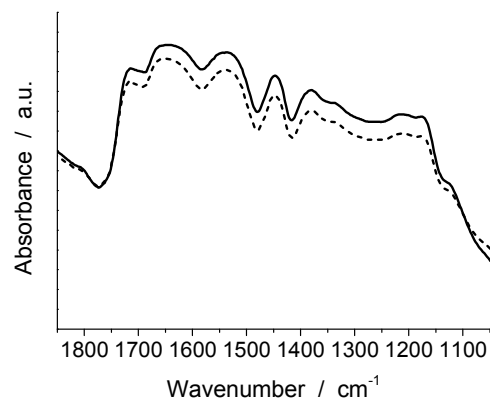


**Figure 8:** Polarized FTIR absorption spectra of aligned PAA/PAH electrospun fiber mats heated to 320 °C. The spectra were acquired with incident infrared light polarized parallel (dashed line) and perpendicular (continuous line) to the fiber axis.

### 3.4 Swelling in response to pH

Previous reports have demonstrated that polyelectrolyte complexes show high dependency on the pH of the aqueous surrounding.<sup>19, 24, 40</sup> In order to gain some insights into the nature of fiber behavior, confocal laser scanning microscopy of their volumetric changes was performed in-situ, in surrounding medium of varying pH levels (Figure 9). Auto-fluorescence of the polyelectrolytes was exploited to increase imaging contrast. Measurements revealed that fiber diameter remained constant above pH 2.6, whereas below 2.6, it displayed a marked increase until pH 1.8, at which point the fibers reached a highly swollen state. At lower pH (e.g., pH 1.6), the fibers disassembled. Fibers at pH 5.5 will serve as reference to the highly swollen state.<sup>19</sup> At pH 1.8, the average increase in fiber diameter and

volume between pH 5.5 and pH 1.8, was found to be 350% and 1225%, respectively. Fiber auto-fluorescence was stronger at pH 5.5, when compared to pH 1.8. The pH range that affected fiber swelling performance was similar to that previously reported for LbL-formed films;<sup>19</sup> 6, 22, 23 nanotube arrays of polyelectrolyte multilayers (PEMs) showed swelling behavior of up to 800% in response to acidic aqueous medium.<sup>19</sup>

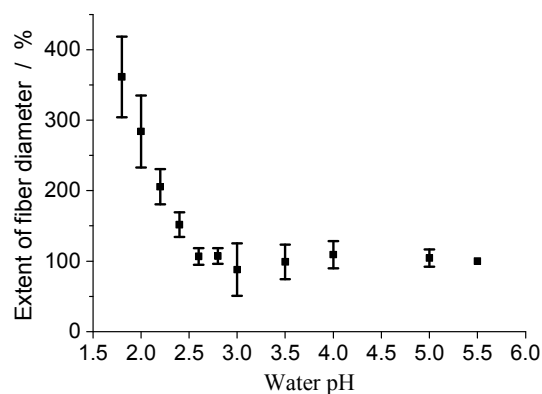


**Figure 9:** Swelling behavior of PAA/PAH fiber mats - diameter of PAA/PAH fibers immersed in water at different pH values.

CLSM images of fibers immersed sequentially in pH 5.5 and pH 1.8 are shown in Figure 10. The volume of fibers immersed at pH 5.5 (Figures 10a, and c) was similar to that of dry fibers, as observed in SEM images (Figure 5). When immersion solution was substituted with water of pH 1.8 (Figure 10b, and d), fibers swelled significantly. Water competency measurements during the swelling process of 10 fiber mats (Figure 10e) showed 50% water adsorption at pH 5.5 and about 1180% water adsorption at pH 1.8 (compared to dry mats). The swelling process was reversible three times; rendering the fiber mats a good candidate as an active material. Attempts to demonstrate swelling-deswelling behavior of cast film were unsuccessful and it dissolved at low pH.

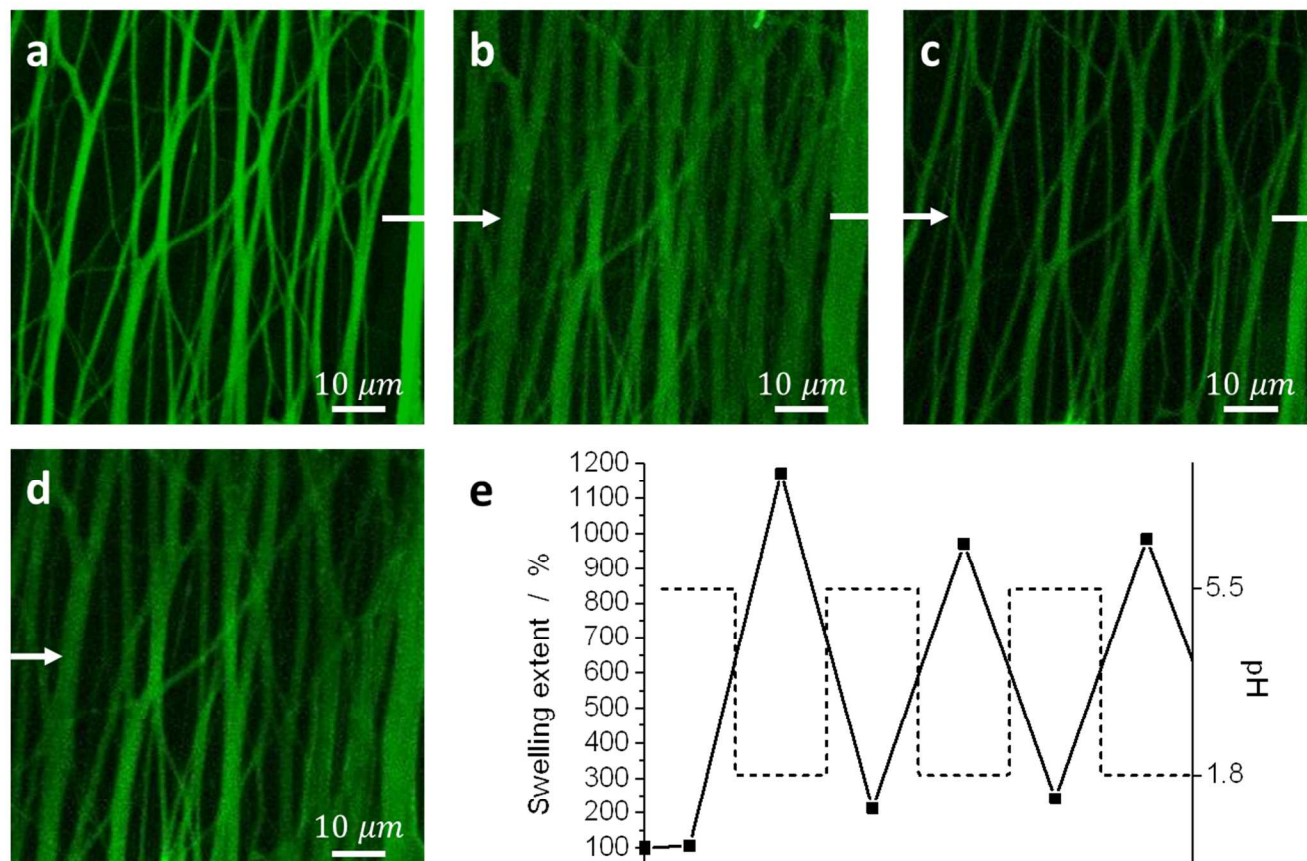


**Figure 10:** Confocal laser scanning microscopy (CLSM) plan-view images of electrospun PAA/PAH fibers sequentially immersed in water at pH 5.5 (a, c) and at pH 1.8 (b, d), and the respective extent of swelling (e).

Cite this: DOI: 10.1039/c0xx00000x

www.rsc.org/xxxxxx

## ARTICLE TYPE

Optical in-situ observation of fibers was used to study the swelling kinetics. Monitoring with high spatial and temporal resolution was enabled due to a special setup which facilitated flushing of liquids (see a movie describing swelling and de-swelling of fiber mast is in the Supplementary information). In order to track the kinetics of the swelling process, fiber diameter was measured as a function of time (see Figure 11). At the beginning, the mean diameter of the non-swollen fibers in water of pH 5.5 was 1.6  $\mu\text{m}$ . Upon replacement of the medium with water of pH 1.8, the mean diameter increased to 6.1  $\mu\text{m}$  within 6 seconds. Replacement of the medium with water of pH 5.5 again, yielded a mean fiber diameter identical to that measured at the starting point, however, required 24 seconds to return to this state. Average swelling and de-swelling rates were approximated as 0.50 and 0.17  $\mu\text{m/s}$ , respectively. The difference in the swelling and de-swelling kinetics may be caused by the difference in rates of diffusion of ions into and out of fibers during changes between low and neutral pH; this point requires further investigation.

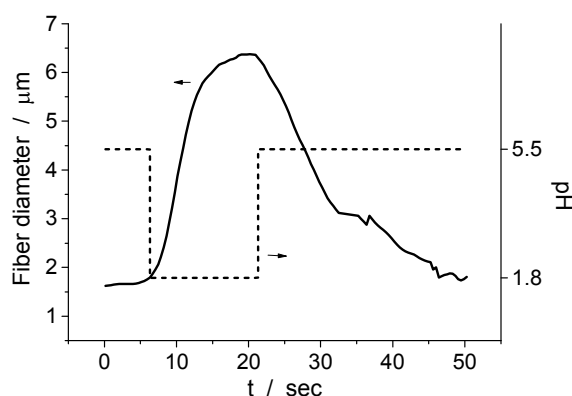
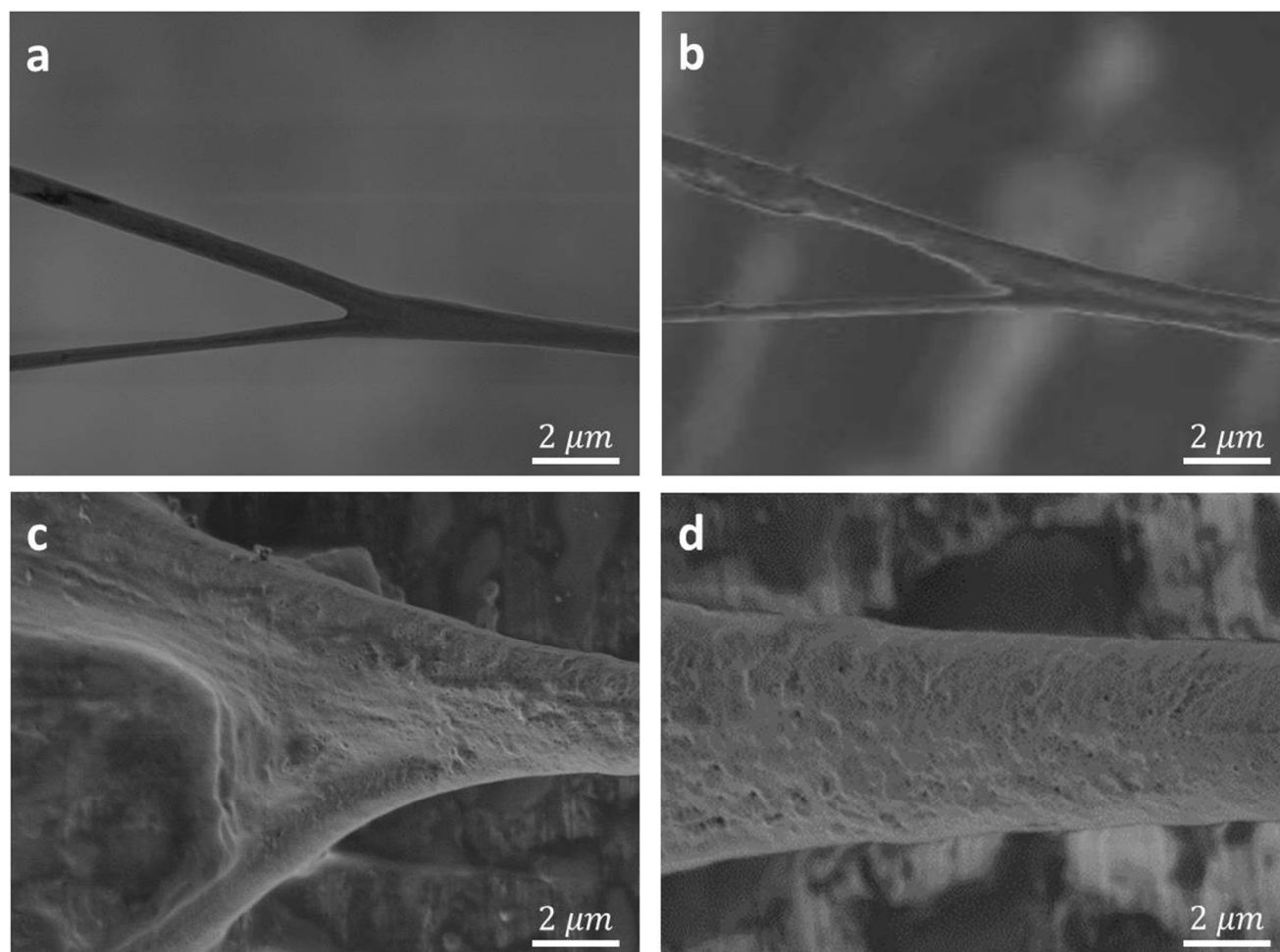


Figure 11: Average diameter of fibers over time under pH change.

Cryo-HRSEM was used to study the morphology of the electrospun fibers. Prior to vitrification, dry electrospun fibers were imaged using HRSEM and showed a uniform, non-porous surface (Figure 12a). Fiber immersion in pH 5.5 followed by cryogenic cooling, using ethane and etching, led to a diameter increase of 110%. However, fibers remained uniform and nonporous, with some irregularities on their surfaces (Figure 12b). Fiber immersion in pH 1.8, followed by cryogenic treatment, led to a 510% increase in diameter, and to generation of many irregularities on the surface, which remained nonporous (Figure 12c). Fibers irradiated for 10 minutes under the microscope demonstrated a rough morphology (Figure 12d), which may be the result of water evaporation from the fiber surface.



**Figure 12:** Cryo-HRSEM of a single electrospun PHA/PAA fiber. (a) Dry state, (b) immersed in water at pH 5.5, (c) immersed in water at pH 1.8, and (d) a larger magnification at pH 1.8 after radiation.

### 3.5 Ionization in response to pH

The major chemical aspect affecting the swelling behavior of the PAA/PAH fiber is the degree of ionization. To determine the degree of ionization, FTIR-ATR spectra of the system in various pH were analyzed.<sup>26</sup> Two distinct peaks were observed for PAA, one at  $1709\text{ cm}^{-1}$ , corresponding to the carboxylic acid, and the other at  $1530\text{ cm}^{-1}$ , which is attributed to the ionized carboxylate (Figure 13a). Since the amine functional group of PAH is mostly protonated in this pH range and does not show any significant change,<sup>41, 42</sup> and due to the challenging nature of PAH peaks characterized by shifting and overlapping with PAA, peak analysis and degree of ionization focused on PAA only.<sup>26</sup> It can be shown that the COOH peak was more significant than the COO<sup>-</sup> up to pH 2.4. However, from pH 2.6, the effect was reversed, and the COOH peak decreased, whereas the carboxylate peak increased dramatically, as most of the carboxylic acid is ionized. From pH 3.5 to pH 5.5, no change was observed.

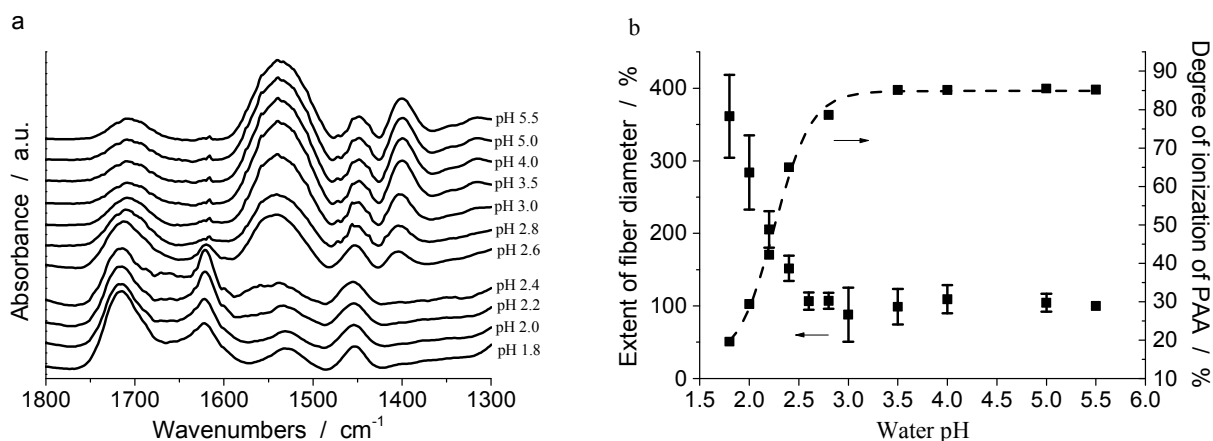


**Figure 13:** (a) FTIR-ATR spectra of PAA/PAH fibers in aqueous solutions of various pH. (b) Estimated degree of ionization of PAA in PAA/PAH fibers and swelling behavior presented as fiber diameter as a function of pH.

The degree of ionization can be represented by the ratio of the  $\text{COO}^-$  peak area to the sum of the peak areas of  $\text{COOH}$  and  $\text{COO}^-$ . While the degree of ionization of PAA increases intensely from pH 1.8 (18% of the groups are ionized) to pH 3.0 (79%), no significant changes in the degree of ionization were observed between pH 3.5 and pH 5.5 (84-85%) (Figure 13b). Previous analyses of pure PAA film showed a low degree of ionization until approximately pH 4.<sup>41, 43, 44</sup> When PAA and PAH are electrospun together, the degree of ionization differs from that of the pure polyelectrolytes due to local environmental effects such as electrostatic field, hydrophobic and chemical effects.<sup>26</sup> First, the local complex between the positive and negative functional groups forms an electrostatic force that lowers the ionization barrier. Secondly, in order to avoid hydrophobic effects in the negatively charged polyelectrolyte, ionization of the PAA is favored. In addition, PAA and PAH may form an acid-base interaction that limits the ionization of PAA.<sup>45</sup> The acid dissociation constant,  $pK_a$  ( $pK_{1/2}$ ), of a cast PAA film ranges from 5.7 to 6.5.<sup>41, 43, 44</sup> When PAA is embedded in PAA/PAH fibers, the ionization of PAA is more favored at lower pH values, thus the  $pK_a$  is lowered. The effective  $pK_a$  of PAA in fibers is roughly 2.3, a dramatic shift from pure PAA. The shift was previously observed and reported for polyelectrolyte complexes<sup>46</sup> and polyelectrolyte multilayers.<sup>26</sup> There is good compatibility between the degree of ionization and the pH-dependent responsive behavior. The effective pH range of the responsive behavior and degree of ionization are identical. The degree of ionization influences the strength of the interactions between the functional groups. When the degree of ionization is low, more hydrogen bonds will form and swelling is enhanced. Conversely, when the PAA functional groups are ionized, more ionic interactions will occur, water diffuse out and the fibers de-swell. Although the degree of ionization of PAA/PAH fibers at a given pH and  $pK_a$  ( $pK_{1/2}$ ) shifts similarly to previously reported results in the literature, the observed responsive behavior, which is also influenced by the assembly packaging and structure,<sup>20</sup> demonstrated alternative performance.

#### 4. Conclusions

The drive to efficiently pack pH-responsive, oppositely charged polyelectrolytes, led us to design quasi 1D-polyelectrolyte structures. Fibers were electrospun from a stoichiometric ratio of PAA/PAH in low-pH homogeneous solution. A 40:60 mixture of an ethanol/water co-solvent was used to obtain uniform fibers. The lower amidation temperature and higher amidation enthalpy in fibers versus the bulk polymer, along with fiber homogeneity, indicate availability of functional groups to interact with one another. Moreover, the fibers demonstrated directionality of the functional groups perpendicular to the fiber axis. These features dictate the uniqueness of the electrospun fiber morphology resulting from its highly confined and aligned structure. The pH of the medium dictated molecular fiber conformation in solution, and was manipulated to demonstrate reversible swelling-deswelling of the electrospun fibers. The threshold of the phenomenon was observed at pH below 2.6. Significant changes of up to 600% in fiber diameter, occurring at a rate of 0.50  $\mu\text{m}/\text{sec}$  under pH 1.8 were observed. The degree of ionization at this pH level was measured to be 17%. From pH 3.5 to neutral, the degree of ionization was at least 79% and de-swelling was observed in this pH range. In contrast, it was impossible to observe the swelling phenomenon of the bulk, due to dissolution of the samples at low pH under the same experimental conditions. The ability to construct tunable confined structures opens a facile avenue toward preparation of novel membranes, tissue engineering scaffolds, drug delivery processes, and sensors.

#### Acknowledgements

We gratefully acknowledge the financial support of the RBNI-Russell Berrie Nanotechnology Institute, the Israel Science Foundation (ISF Grant 770/11), and the National Research Foundation (R-398-001-065-592) of Singapore in the framework of the Regenerative Medicine Initiative.

## Notes and references

<sup>a</sup> Russell Berrie Nanotechnology Institute, Technion-Israel Institute of Technology, Haifa, 32000, Israel. E-mail: morboas@tx.technion.ac.il

<sup>b</sup> Faculty of Mechanical Engineering, Technion-Israel Institute of Technology, Haifa, 32000, Israel.

<sup>c</sup> Institute of Fundamental Technological Research of Polish Academy of Sciences, Pawinskiego 5B, 02-106 Warsaw, Poland

† Electronic Supplementary Information (ESI) available: [details of any supplementary information available should be included here]. See DOI: 10.1039/b000000x/

1. R. Chollakup, W. Smitthipong, C. D. Eisenbach and M. Tirrell, *Macromolecules*, 2010, **43**, 2518-2528.
2. M. Hara, *Polyelectrolytes: science and technology*, Marcel Dekker, New York, 1993.
3. A. Drogoz, L. David, C. Rochas, A. Domard and T. Delair, *Langmuir*, 2007, **23**, 10950-10958.
4. J. Kötz, S. Kosmella and A. Ebert, *Acta Polymerica*, 1992, **43**, 313-319.
5. A. A. Lazutin, A. N. Semenov and V. V. Vasilevskaya, *Macromolecular Theory and Simulations*, 2012, **21**, 328-339.
6. G. Decher, *Science*, 1997, **277**, 1232-1237.
7. G. Decher, J. D. Hong and J. Schmitt, *Thin Solid Films*, 1992, **210-211, Part 2**, 831-835.
8. Y. Ma, J. Dong, S. Bhattacharjee, S. Wijeratne, M. L. Bruening and G. L. Baker, *Langmuir*, 2013, **29**, 2946-2954.
9. D. H. Reneker, A. L. Yarin, E. Zussman and H. Xu, *Adv. Appl. Mech.*, 2007, **41**, 43-195.
10. D. H. Reneker and A. L. Yarin, *Polymer*, 2008, **49**, 2387-2425.
11. I. Greenfeld, A. Arinstein, K. Fezzaa, M. H. Rafailovich and E. Zussman, *Physical Review E*, 2011, **84**, 041806.
12. I. Greenfeld, K. Fezzaa, M. H. Rafailovich and E. Zussman, *Macromolecules*, 2012, **45**, 3616-3626.
13. S. Curgul, K. J. Van Vliet and G. C. Rutledge, *Macromolecules*, 2007, **40**, 8483-8489.
14. A. Arinstein and E. Zussman, *Journal of Polymer Science Part B-Polymer Physics*, 2011, **49**, 691-707.
15. A. Arinstein, M. Burman, O. Gendelman and E. Zussman, *Nature Nanotechnology*, 2007, **2**, 59-62.
16. A. Camposeo, I. Greenfeld, F. Tantussi, S. Pagliara, M. Moffa, F. Fuso, M. Allegrini, E. Zussman and D. Pisignano, *Nano Letters*, 2013, **13**, 5056-5062.
17. E. V. Skorb and H. Möhwald, *Advanced Materials*, 2013, **25**, 5029-5043.
18. M. Xu and J. A. Lewis, *Langmuir*, 2007, **23**, 12752-12759.
19. K.-K. Chia, M. F. Rubner and R. E. Cohen, *Langmuir*, 2009, **25**, 14044-14052.
20. S. W. Cranford and M. J. Buehler, *Macromolecules*, 2012, **45**, 8067-8082.
21. P. G. Degennes, P. Pincus, R. M. Velasco and F. Brochard, *Journal De Physique*, 1976, **37**, 1461-1473.
22. J. L. Barrat and J. F. Joanny, in *Advances in Polymer Physics, Polymer Systems*, eds. I. Prigogine and S. A. Rice, John Wiley & Sons Inc., 1996, vol. XCIV, p. 67.
23. L. Han, J. Yin, L. Wang, K.-K. Chia, R. E. Cohen, M. F. Rubner, C. Ortiz and M. C. Boyce, *Soft Matter*, 2012, **8**, 8642-8650.
24. J. A. Hiller, J. D. Mendelsohn and M. F. Rubner, *Nat Mater*, 2002, **1**, 59-63.
25. L. Shao and J. L. Lutkenhaus, *Soft Matter*, 2010, **6**, 3363-3369.
26. J. Choi and M. F. Rubner, *Macromolecules*, 2005, **38**, 116-124.
27. S. S. Shiratori and M. F. Rubner, *Macromolecules*, 2000, **33**, 4213-4219.
28. S. W. Cranford, C. Ortiz and M. J. Buehler, *Soft Matter*, 2010, **6**, 4175-4188.
29. I. Greenfeld, A. Arinstein, K. Fezzaa, M. H. Rafailovich and E. Zussman, *Physical Review E*, 2011, **84**, 041806.
30. D. Reith, H. Meyer and F. Müller-Plathe, *Macromolecules*, 2001, **34**, 2335-2345.
31. H. V. Sæther, H. K. Holme, G. Maurstad, O. Smidsrød and B. T. Stokke, *Carbohydrate Polymers*, 2008, **74**, 813-821.
32. A. Theron, E. Zussman and A. L. Yarin, *Nanotechnology*, 2001, **12**, 384-390.
33. A. F. Xie and S. Granick, *Macromolecules*, 2002, **35**, 1805-1813.
34. W. M. Huang, H. B. Lu, Y. Zhao, Z. Ding, C. C. Wang, J. L. Zhang, L. Sun, J. Fu and X. Y. Gao, *Materials & Design*, 2014, **59**, 176-192.
35. Y. Hayashi, M. Ullner and P. Linse, *Journal of Physical Chemistry B*, 2003, **107**, 8198-8207.
36. A. Chunder, S. Sarkar, Y. B. Yu and L. Zhai, *Colloids and Surfaces B-Biointerfaces*, 2007, **58**, 172-179.
37. S. Dubinsky, G. S. Grader, G. E. Shter and M. S. Silverstein, *Polymer Degradation and Stability*, 2004, **86**, 171-178.
38. F. Caruso, D. N. Furlong, K. Ariga, I. Ichinose and T. Kunitake, *Langmuir*, 1998, **14**, 4559-4565.
39. Z. Yang, X. Lei, J. Wang, R. Luo, T. He, H. Sun and N. Huang, *Plasma Processes and Polymers*, 2011, **8**, 208-214.
40. L. A. Connal, Q. Li, J. F. Quinn, E. Tjipto, F. Caruso and G. G. Qiao, *Macromolecules*, 2008, **41**, 2620-2626.
41. A. I. Petrov, A. A. Antipov and G. B. Sukhorukov, *Macromolecules*, 2003, **36**, 10079-10086.
42. M. M. Fang, C. H. Kim and T. E. Mallouk, *Chemistry of Materials*, 1999, **11**, 1519-1525.
43. L. Bromberg, *Journal of Physical Chemistry B*, 1998, **102**, 10736-10744.
44. O. E. Philippova, D. Hourdet, R. Audebert and A. R. Khokhlov, *Macromolecules*, 1997, **30**, 8278-8285.
45. L. Bromberg, M. Temchenko and T. A. Hatton, *Langmuir*, 2003, **19**, 8675-8684.
46. T. K. Bronich, A. V. Kabanov, V. A. Kabanov, K. Yu and A. Eisenberg, *Macromolecules*, 1997, **30**, 3519-3525.